Multiparameter-based photosynthetic state transitions of single phytoplankton cells

Paul David Harris[1], Nadav Ben Eliezer[2], Nir Keren[2,3,*], Eitan Lerner[1,4,*]

[1]Department of Biological Chemistry, The Alexander Silberman Institute of Life Sciences, The Hebrew University of Jerusalem; Jerusalem, Israel, 9190401.

[2]Department of Plant Sciences, The Alexander Silberman Institute of Life Sciences, The Hebrew University of Jerusalem; Jerusalem, Israel, 9190401.

[3]The Interuniversity Institute for Marine Sciences, Eilat, Israel.

[4]The Center for Nanoscience and Nanotechnology, The Hebrew University of Jerusalem; Jerusalem, 9190401, Israel.

*Corresponding authors: nir.ke@mail.huji.ac.il;eitan.lerner@mail.huji.ac.il

Abstract

Fluorescence emitted by light-harvesting pigments responds to the physiological state of phytoplankton. We developed a time resolved system to monitor fluorescence from single cells. It captures multiple spectral channels and fluorescence lifetimes, eliminating ensemble averaging of bulk experiments. Tracking the diurnal cycles of three phytoplankton species, we uncover each species segregation into multiple distinct cell states, a feature previously hidden in bulk measurements. We also tested their response to light-intensity perturbations, and determined each species unique acclimation strategy involving transition between distinct cell subpopulations. This approach will be useful for characterizing natural phytoplankton population responses to environmental conditions, aiming for a better understanding of their acclimation strategies and the effects of global climate changes.

One sentence summary

Photophysiological phytoplankton cell states are uncovered at the multiparameter single cell level.

Main Text

Current limits of experimental phytoplankton photophysiology

Light is the major source of energy for life on Earth. However, it is a dilute and often limiting resource (*1*). At its peak, sunlight reaches levels of about 2.5×10^3 moles of photosynthetically active photons m^{-2} s^{-1} (photosynthetically active radiation, PAR, 400-700 nm) and in most aquatic environments photosynthesis takes place at much lower light intensities. Moreover, light in the ocean changes significantly over horizontal, vertical, and temporal scales (*2*). When considering the vertical dimension, light intensity decreases exponentially with depth in the water column. In addition, light quality changes as a function of depth and so does the amount and type of particulate matter found within the water. The dynamic nature of light within these environments poses significant challenges to photosynthesis. Low light intensities necessitate efficient light harvesting, while high light intensities can be damaging and may require mechanisms for dissipation of excess energy (*3*). Phytoplankton in a vertical mixing water column may be exposed to a gradient of light intensities and qualities over the course of a day (*4*).

A diverse range of marine photoautotrophs have evolved to meet these challenges through unique adaptations of the photosynthetic apparatus. The form and function of the photosynthetic electron transport chain is, overall, uniform across the oxygenic photosynthetic species. Light harvesting complex (LHC) systems, on the other hand, diverge significantly between phytoplankton groups and determine the range of light intensity and quality niches they can inhabit (*5*). In this study, we focused on "red lineage" oceanic phototrophs (*6*). Marine prokaryotic *Synechococcus* species harvest light through elaborately-pigmented cytoplasmic/stromal phycobilisomes (PBSs). Their complex pigmentation pattern provides a wealth of spectroscopic handles for their function (Fig. 1, Table S1). Red algae are the evolutionary progeny of an endosymbiosis event with a *Synechococcus* type cyanobacteria that also use PBSs (*6*). The recent resolution of the complete *Porphyridium purpureum* red algae PBS structure (*7*) facilitated the ability to study their structure-function relationship (*8*). This massive structure contains 1,598 resolved chromophores. Dinoflagellates are secondary endosymbionts, with an ancestral red alga (*6*). They abandoned PBS-type LHCs to utilized thylakoid-embedded chlorophyll *a*/*c* LHCs (apcCP) (*9*, *10*) and lumen chlorophyll-peridinin PCP antennas (*11*–*13*) (Fig. 1, Table S1). There is a large diversity in photosynthetic lifestyles and light harvesting strategies among dinoflagellates (*14*). In this study we worked with *Prorocentrum micans*, a dinoflagellate species in which large dynamic changes in both apcCP and PCP functions were demonstrated (*15*).

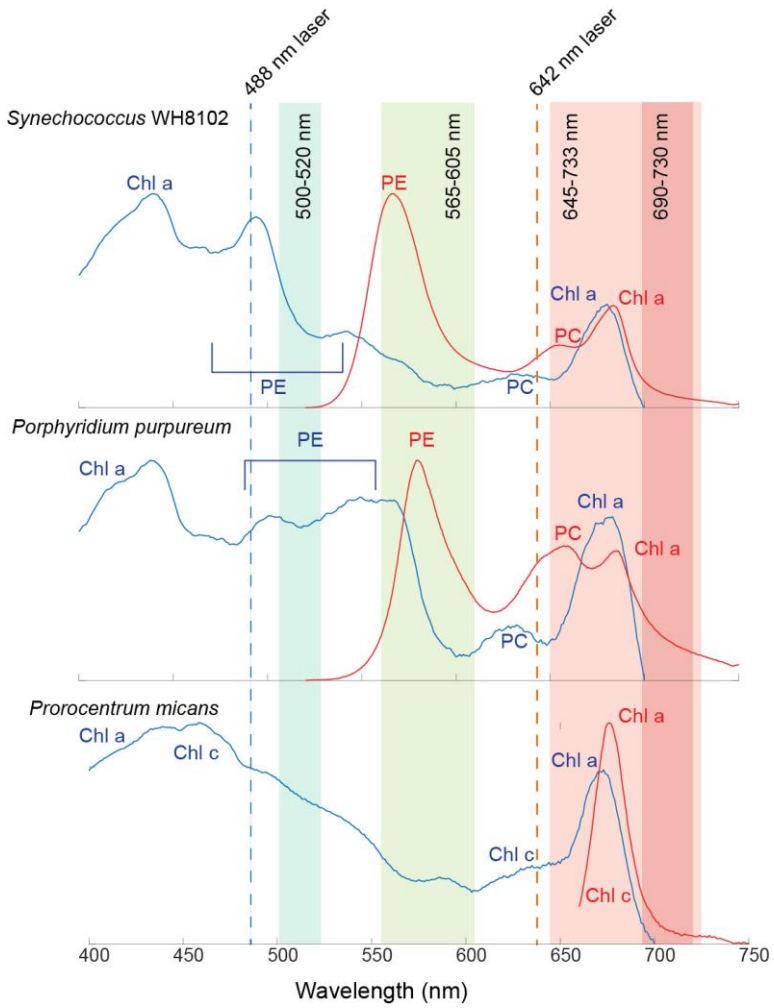

Fig. 1: Spectra of algal species, and optical layout

The algal species used in this study: (i) *Synechococcus* WH8102 (*Syn*. WH8102), (ii) red algae *Porphyridium purpureum* (*P. purp*), and (iii) dinoflagellate *Prorocentrum micans* (*P. micans*). The absorption (blue) and the fluorescence (red) spectra are shown for each species. The spectra are normalized, and the major chromophore spectral component peaks are indicated (additional information in table S1). The time-resolved single cell detection system is driven by two pulsed excitation sources at 488 and 642 nm (blue and orange vertical dashed lines, respectively), and emitted photons are being detected using four detectors for four separate spectral ranges (cyan, green, light red and dark red shades; additional information in tables 1, 2, S1).

The potential of multiparameter single cell photon counting experiments

In an oceanographic context, fluorescence intensity-based measurements are commonly used to infer and interpret photophysiology. Intensity-based measurements are sensitive and straightforward, while time-resolved measurements are rarely used, however fluorescence lifetime measurements provide unique insights on the transfer of absorbed energy from antenna systems to PSII. Briefly, light energy absorbed by LHC or PBS systems can be transferred to reaction centers and transformed into a form available for cellular processes. Alternatively, the excitation energy can either be dissipated as heat or radiatively-emitted as fluorescence. Fluorescence lifetime measurements can provide direct information on the quantum yields of these energy de-excitation processes, and therefore can close the energetic budget for the quantum yield of photochemistry (for a detailed discussion see Gorbunov and Falkowski (*1*)).

Few studies of phytoplankton have applied time-resolved fluorescence studies in a bulk spectroscopic approach (e.g., (*16*–*18*)). In bulk spectroscopy, the fluorescence lifetime data is ensemble-averaged over all contributing fluorophores present in the subpopulations of all cells in the detection volume. In this study we take this approach one step further towards disentangling fluorescence parameters: intensity, brightness (i.e., photon rate) and lifetimes, originating from single cells and their grouping into cell-based subpopulations. In addition, with such rich data arising from multiple excitation and emission band combinations it is only natural to attempt grouping cells in multidimensional parameter space into unique subpopulation signatures that may otherwise be hidden.

Using a diffraction-limited confocal volume, it is possible to construct images with subcellular spatial resolution of time-resolved fluorescence. When the confocal volume is scanned across spatially-confined cells, this method is known as fluorescence lifetime imaging (FLIM) (*19*). FLIM was used for imaging a diverse range of photosynthetic cells, including cyanobacteria, green algae and plants (*20*–*25*). Importantly, it is also possible to detect fluorescence from single organisms, one at a time, in flow-based techniques like flow cytometry (*26*). While most flow-based measurements do not provide sub-cellular resolution as in FLIM, they compensate by providing higher-throughput detection of multiple single cell organisms (*26*).

Here, we sought to examine the heterogeneity within phytoplankton from the red lineage, including potential cell-states based on photosynthetic parameters and the related cell-state transition dynamics as an acclimation response to varying light conditions. Promptly, we developed a new confocal-based flow experimental scheme capable of measuring fluorescence parameters driven by multiple pulsed excitation sources and multiple emission bands, from individual cells, simultaneously characterizing them for both excitation and emission profiles with time-resolved fluorimetry. We resolved individual cells as bursts of detected fluorescence photons flowing through a microfluidic channel and probed with multiple confocal-based pulsed-interleaved excitation sources and fluorescence detected in multiple spectral channels (Fig. 2, Tables 1, 2, Materials and Methods). With the capacity to measure thousands of cells per hour, we characterized two light acclimation processes: (i) diurnal cycles, and (ii) response to an abrupt increase in

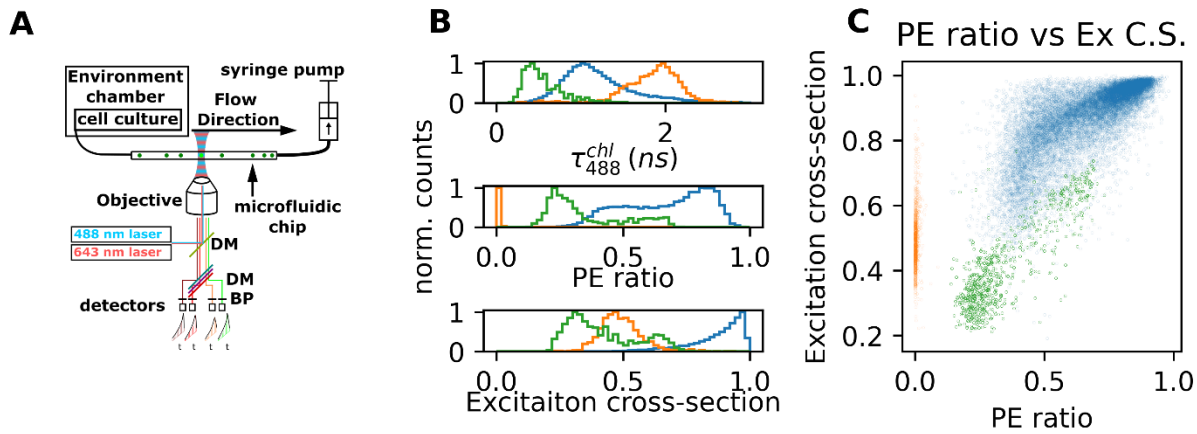

Fig. 2. Flow-based single cell measurements

A) Diagram of the method. A cell culture is kept in an environmental chamber next to the microscope, with a culture flask containing the phytoplankton. An FPLC tube connects the culture to a microfluidic channel embedded on top of a microscope glass slide, fixed atop the microscope stage, with the outlet connected to a syringe pump, which is used to induce flow of organisms through the microfluidic channel. Pulsed-interleaved laser excitations at two wavelengths are focused as a diffraction-limited spot inside the microfluidic channel, and fluorescence photons are collected through the same objective lens, filtered, and cleaned through a pinhole. Then, the signal is chromatically split using dichroic mirrors (DM), further optically cleaned using bandpass (BP) filters and then detected in four spectral bands using single photon counting detectors. Distinct parameter signatures of different cell types are observed in B) 1D histograms of single-cell values along three selected parameters, and C) 2D scatter plot of a pair of selected parameters.

light intensity. Our results uncover the cell-states that phytoplankton populate, their transition dynamics and their efficiencies, which were otherwise masked by ensemble averaging and the use of minimal sets of fluorescence parameters.

Table 1: Selected mean fluorescence lifetime parameters

$\lambda_{ex.}$(nm)[1]	$\lambda_{detection}$ range (nm)[2]	***Syn. WH8102* and *P. purp***	***P. micans***
488	566-605	PE ($\boldsymbol{\tau_{488}^{PE}}$)	-
	645-733	PE-excited and energy transfer to *chl a*, APC, PC ($\boldsymbol{\tau_{488}^{PC+APC+chl}}$)	$\boldsymbol{\tau_{488}^{chl\ a+c}}$
	690-730	PE-excited and energy transfer to *chl a* ($\boldsymbol{\tau_{488}^{chl}}$)	$\boldsymbol{\tau_{488}^{chl\ a}}$
642	645-733	*chl a*, APC, PC ($\boldsymbol{\tau_{642}^{PC+APC+chl}}$)	$\boldsymbol{\tau_{642}^{chl\ a+c}}$
	690-730	*chl a* ($\boldsymbol{\tau_{642}^{chl}}$)	$\boldsymbol{\tau_{642}^{chl\ a}}$
488 & 642	690-730	The mean *chl a* lifetime difference between PE-excited and energy transfer to *chl a* vs. more directly-excited *chl a* ($\boldsymbol{\tau_{488}^{chl} - \tau_{642}^{chl}}$, **or,** $\boldsymbol{\Delta\tau^{chl}}$)	-

[1] Pulsed laser excitation wavelength.
[2] Fluorescence detection wavelength range.

Table 2: Selected brightness ratio parameters

Calculated parameter	*Syn. WH8102* and *P. purp*	*P. micans*
$\frac{[Ex: 488, Em: (565-602)]}{[Ex: 488, Em: (565-605)\ \&\ (645-733)]}$	**PE ratio** • PE emission brightness divided by the total emission recorded in the two channels covering emission from photosynthetic pigments.	-
$\frac{[Ex: 488, Em: (645-733)]}{[Ex: 488, Em: (565-605)\ \&\ (645-733)]}$	**PC+APC+chl ratio** • Combined emission from PC, APC and *chl* in PBS and PSII, divided by total emission in the two channels covering emission from photosynthetic pigments.	
$\frac{[Ex: 488, Em: (690-730)]}{[Ex: 488, Em: (565-605)\ \&\ (645-733)]}$	***chl* ratio** • *chl a* emission brightness divided by the total emissions recorded in two channels covering emission from photosynthetic pigments.	
$\frac{[Ex: 488, Em: (645-733)\ \&\ (690-730)]}{[Ex: 488\ \&642, Em: (645-733)\ \&\ (690-730)]}$	**PBS cross-section (PBS C.S.)** • Emission brightness originating from 488 nm excitation in the *chl* channels divided by the sum of brightnesses resulting from excitation with both 488 and 642 nm lasers.	**Excitation cross-section (Ex C.S.)** • Both 488 and 642 nm excite both *chl a*/c.
$[Ex: 488, Em: (500-520)]$ (counts s^{-1})	**Apparent reduced Flavin content (ARFC)** • Some reduced flavins have emission in this spectral band.	

Synechococcus cell state transitions in diurnal cycles

Using pulsed-interleaved laser excitations at two wavelengths with four detection windows generates a large parameter space for each of the three organisms tested in this study (Figs. 1, 2, Tables 1, 2). Importantly, data collected from the different species are represented in different areas of this parameter space. This generates a clear separation of the different species in parameter space that can be easily observed in plots of selected parameters (Fig. 2, B, C).

To establish the reliability and potential of our method for reporting photophysiology at the single cell level, we choose to start by characterizing the diurnal cycle of *Synechococcus* WH8102 (*Syn.* WH8102) (Fig. 3). Daytime light intensity was set to mimic the natural light that penetrates marine water columns (60 µmol photons m^{-2} s^{-1} of blue LED light) (*27*), which is considered moderate for *Syn.* WH8102 (*28*). Small variations in mean fluorescence lifetime parameters were observed throughout the diurnal cycle (Fig. 3,

A-C; table S2). Performing the experiment on a single-cell basis provides means of attaining cell-based parameter distributions, and hence the results are presented as parameter-based histograms as a function of time within the diurnal cycle. Examining hour-by-hour histograms of photon bursts revealed that while the distributions of mean fluorescence lifetime parameters typically showed a single clear maximum, they visually did not follow a simple Gaussian distribution, which would otherwise be expected from shot noise and central limit considerations for a single population of parameter values, suggesting at least a two-state heterogeneity of cells in the culture (Fig. 3; figs. S1-5). Fits to multiple Gaussian models using the F-test to determine the best-fit model with a minimal number of subpopulations similarly indicate multiple subpopulations are present (see Materials and Methods).

The strength of coupling between PBS and PSII was assessed through the burst-wise difference in mean fluorescence lifetime of *chl a* between excited through energy transfer from PE and excited more directly *chl a*, $\tau_{488}^{chl} - \tau_{642}^{chl}$. No significant diurnal changes were detected in this parameter (Fig, 3, D), indicating that the diurnal changes observed in the individual parameters, under this light intensity, do not dramatically influence the coupling strength between PBS and PSII.

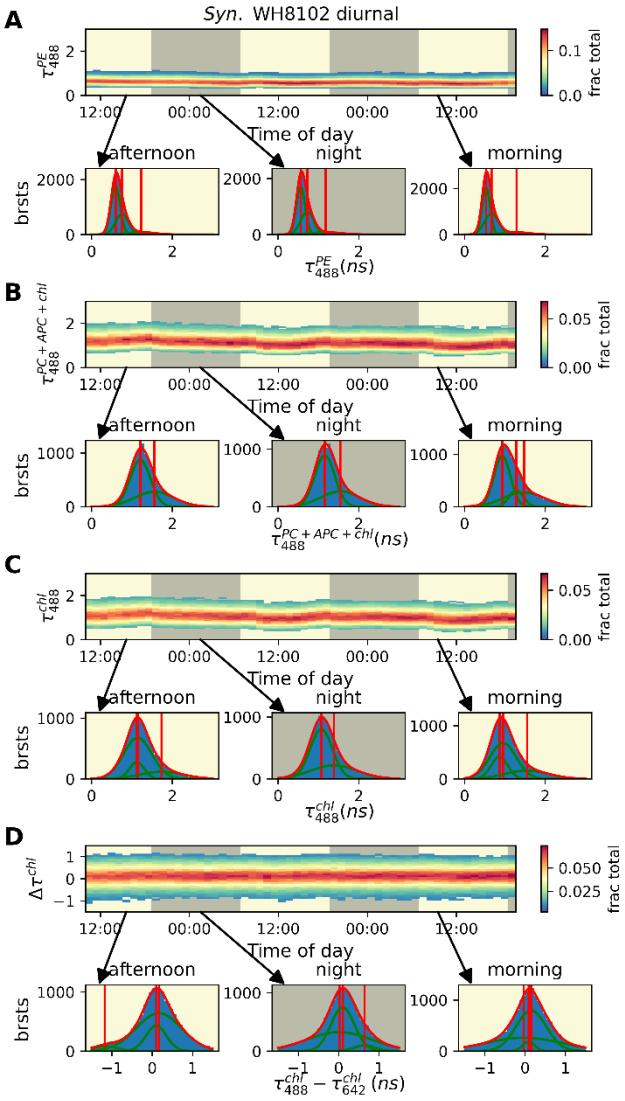

Fig. 3. Mean fluorescence lifetime parameters in diurnal cycle of *Syn.* WH8102

Kymographs show changes in populations of mean fluorescence lifetime or lifetime difference parameters plotted along the vertical axis, and time within the diurnal cycle along the horizontal axis. Day and night are indicated by yellow and gray backgrounds, respectively. Bursts of individual organisms are grouped into hour-long bins. Plots below the kymographs show select histograms of burst mean fluorescence lifetime or lifetime difference values. Vertical lines in histograms represent the centroids of Gaussians when performing a sum-of-multiple-Gaussians model fitting to the data and selecting the best-fit model based on F-test, red line represents the fitted model, while green lines represent the Gaussians with each model. The A) mean fluorescence lifetime of τ_{488}^{PE} streams (i.e., direct excitation of PE), B) mean fluorescence lifetime of τ_{488}^{chl} (i.e., excitation of *chl a* through PE excitation and energy transfer) C) mean fluorescence lifetime of τ_{488}^{chl} (i.e., excitation of *chl a* through PE excitation and energy transfer), and D) fluorescence lifetime difference $\tau_{488}^{chl} - \tau_{642}^{chl}$ (i.e., the difference between mean fluorescence lifetimes of *chl a*, following PE excitation and energy transfer to *chl a* versus more directly excited *chl a*), are shown. This fluorescence lifetime difference reflects the rate of nonradiative energy transfer to *chl a* in PSII through the PBS (PE, PC, APC).

We next turn to examine the spectral characteristics of the emission brightness parameter of PE (PE ratio, Table 2), where heterogeneity is found to be pronounced. Hour-by-hour histograms appear as two centrally-distributed subpopulations (Fig. 4, A-C; figs. S6-S8). The maxima of both subpopulations shifted slightly throughout the diurnal cycle, with more PE emission during daylight compared with nighttime. However, the shift throughout the day is smaller than the separation between the two subpopulations. When the *Syn. WH8102* PBS cross-section (Table 2) is correlated with the PE ratio, a more complex pattern emerges (fig. S9). There are indeed two distinct subpopulations of cells, which show two distinct PE ratio:PBS cross-section correlations. This indicates that under normal conditions the cells populate two states with distinct photophysiological behaviors. Finally, the distribution of the apparent reduced flavin content parameter (ARFC, Table 2) was found to be relatively constant throughout the diurnal cycle. The diurnal changes observed in mean fluorescence lifetime and in brightness-based parameters reflects a small degree of daytime reduction in photochemical yields that is expected under the light intensity used (*28*). Red algae, which use a similar yet not identical PBS LHC, show clear diurnal oscillations in mean fluorescence lifetime parameters (fig. S10). In PE ratio, *chl* ratio and PBS cross-section parameters, hour by hour histograms appear as two centrally distributed subpopulations providing clear evidence for two distinct cell states, similar to those observed in *Syn.* WH8102 (fig. S11).

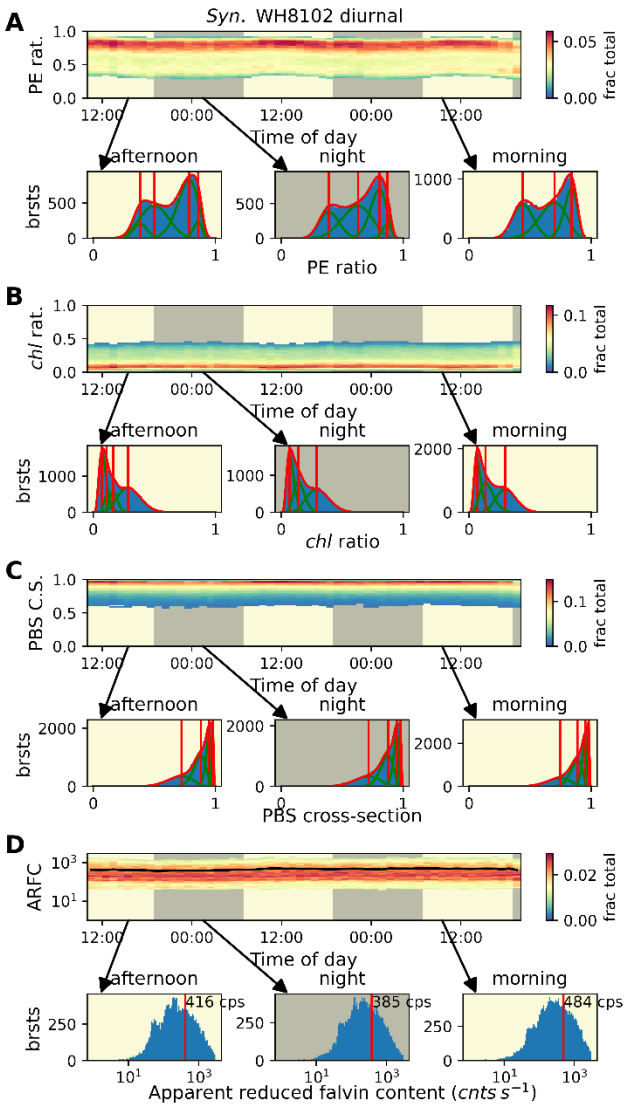

Fig. 4. Brightness ratio parameters in diurnal cycle of *Syn.* WH8102

Kymographs and selected histograms of brightness and brightness ratio parameters. Displayed in the same style as Fig. 3. Bursts of individual cells are grouped into hour-long bins. Day and night are indicated by yellow and gray backgrounds respectively. Histograms of bursts below kymographs show select hour periods of brightness ratio parameters with fittings to models of a sum-of-multiple-beta-distributions, with the best-fit model selected by the F-test. Vertical lines in histograms represent the centroids of beta distributions when performing a sum-of-multiple-beta-distributions model fitting to the data and selecting the best-fit model based on F-test, red line represents the fitted model, while green lines represent the beta distributions within each model. The (A) PE ratio (relative proportion of emission from PE), (B) *chl* ratio (i.e., relative emission from *chl a*), (C) PBS cross section (relative fluorescence from 488 nm excitation), and (D) apparent reduced flavin content (i.e., brightness of emission in flavin channel), are shown. In histograms of apparent reduced flavin content the mean of raw data is reported as a vertical red line, instead of fitting the to any type of distribution.

Synechococcus cell-state transitions in response to light perturbation

Next, we sought to challenge the photosynthetic apparatus by applying a light intensity perturbation. We repeated our diurnal cycle experiment, but on the second day, from 9:00 – 11:00 am, the cells were subjected to a ~5-fold increase in light intensity, which we refer to as a "light jump". This light increase is still within the physiological range of reactions for these cells (*28*). Changes in parameter values were observed within the first hour of the light jump onset (Fig. 5, figs. S12-S20). Since the cells spend ~30 minutes in the dark while in transit from the culture flask to the confocal detection within the microfluidic channel, the response occurs within the practical time resolution of the experiment, which we substantiated using analogous bulk spectral measurements (fig. S21). Changes were most pronounced in mean fluorescence lifetime parameters, where a subpopulation of longer $\boldsymbol{\tau_{488}^{PE}}$ values appears with a value of ~1.6 ns (Fig. 5, A-C, figs. S12-S16). Two distinct subpopulations are present for all mean fluorescence lifetime parameters (Fig. 5, A-C), indicating that mean fluorescence lifetimes do not change continuously, but rather each cell belongs either to pre- or post-light jump subpopulations. Intermediate mean fluorescence lifetime values are conspicuously absent, indicating almost no cells exhibit intermediate values of this parameter. Interestingly, the long mean fluorescence lifetime subpopulation persists for ~12 hours post light jump. Upon return to normal light intensity, the relative fraction of the long mean fluorescence lifetime subpopulation gradually decreases, yet mean fluorescence lifetime values intermediate to the two subpopulations are still not observed.

After the light jump, another effect is observed in the heretofore very stable behavior of the $\tau_{488}^{chl} - \tau_{642}^{chl}$ parameter. In the hours immediately following the light jump, an increase is observed in this parameter, which gradually decreases post light jump (Fig. 5, D). This suggests that much of the observed increase in mean fluorescence lifetimes is due to the reduction in the efficiency of nonradiative energy transfer due to decoupling of PBS from PSII.

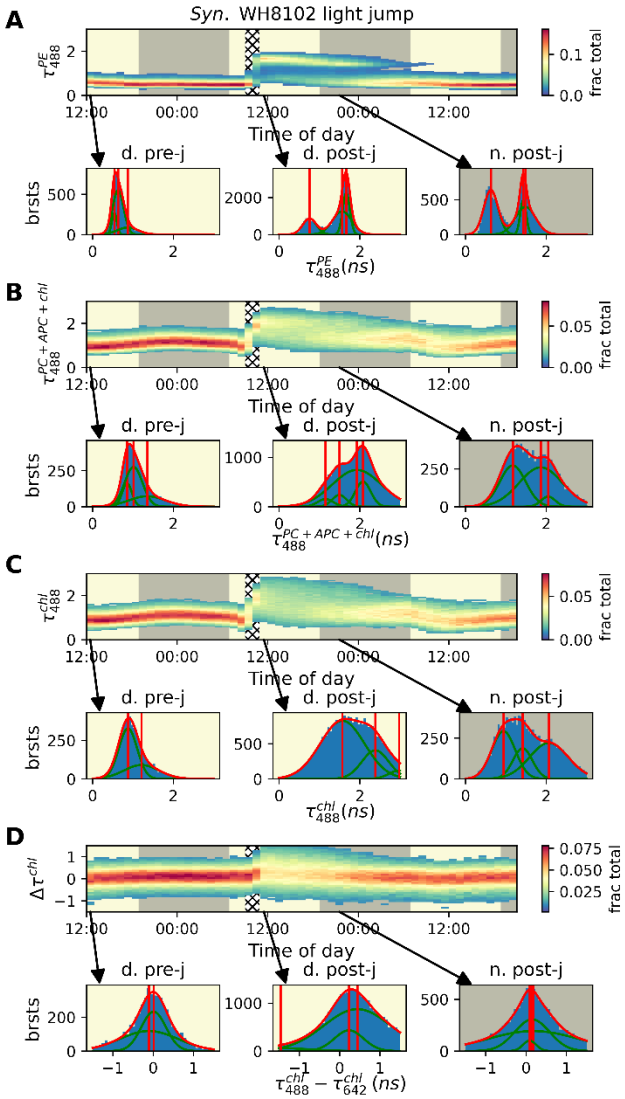

Fig. 5. Mean fluorescence lifetime parameters of *Syn.* WH8102 in response to light perturbation

(Organized identically to Fig. 3) Kymographs show changes in populations of mean fluorescence lifetime or lifetime difference parameters plotted along the vertical axis, and time within the diurnal cycle along the horizontal axis. Day and night are indicated by yellow and gray backgrounds respectively, and the period of the light perturbation is indicated by gridded background. Bursts of individual organisms are grouped into hour-long bins. Plots below the kymographs show select histograms of burst mean fluorescence lifetime or lifetime difference values. Vertical lines in histograms represent the centroids of Gaussians when performing a sum-of-multiple-Gaussians model fitting to the data and selecting the best-fit model based on F-test, red line represents the fitted model, while green lines represent the Gaussians with each model. The A) mean fluorescence lifetime of τ_{488}^{PE} streams (i.e., direct excitation of PE), B) mean fluorescence lifetime of $\tau_{488}^{PC+APC+chl}$ (i.e., excitation of PC, APC, and *chl* through PE excitation and energy transfer), C) mean fluorescence lifetime of τ_{488}^{chl} (i.e., excitation of *chl* through PE excitation and energy transfer), and D) fluorescence lifetime difference $\tau_{488}^{chl} - \tau_{642}^{chl}$ (i.e., the difference between mean fluorescence lifetimes of *chl a*, following PE excitation and energy transfer to *chl a* versus more directly excited *chl a*) are shown. This fluorescence lifetime difference reflects the rate of nonradiative energy transfer to *chl* in PSII through the PBS (PE, PC, APC).

Examination of the PE ratio histograms of the same time period shows that the subpopulation of cells exhibiting stronger *chl a* emission (i.e., lower PE ratio values; fig. S16) decreases in amplitude. The centroid of the high PE ratio subpopulation increased slightly during the light jump, while that of the lower PE ratio showed a more pronounced increase in its centroid, from a mean of ~0.4 during daylight before the light jump, to a mean of ~0.6 after the light jump, respectively (fig. S21, A, B). Bulk fluorescence measurements exhibit a small yet observable decrease in the intensity of the corresponding peaks (fig. S20).

By examining the PE ratio histograms filtered by $\boldsymbol{\tau_{488}^{PE}}$ values (fig. S22), it becomes clear that the long $\boldsymbol{\tau_{488}^{PE}}$ subpopulation after the light jump originates from transitions of cells from both basal short $\boldsymbol{\tau_{488}^{PE}}$ subpopulations. For a full description of this analysis, see Supplementary Materials. Additionally, the apparent reduced flavin species content rises due to the light jump, and slowly returns to pre-light jump values by the beginning of the next day (fig. S22, C, D).

The intracellular meaning of correlated state transitions

Our flow-based data establishes switching between distinct cells-states observed through multiple fluorescence-based parameters. However, the burst-based parameter values may serve as ensemble averages of different photosynthetic complexes within each cell. To test this, we further verified the above flow-based single-cell observations by cell imaging. We perform pulsed-interleaved excitation (PIE) (*29*) coupled with FLIM, PIE-FLIM (*30*), acquisitions of cyanobacteria spatially-confined in agarose (Fig. 6). Performing PIE-FLIM allows us to probe the fluorescence parameters we use in the flow-based measurement, also in imaging mode. We tested if pixel-wise parameters inside the cells also distribute into distinct groups of fluorescence values. Our results indicate that Syn. WH8102 cells group into two distinct predominant subpopulations for many of our fluorescence-based parameters. Additionally, we used the white light of the microscope, typically used for recording bright field images, as our source for a light jump. In these “light jump” experiments, we are able to show the increase in mean fluorescence lifetime parameter values 30 min after the light jump event, as well as smaller changes in intensity ratio parameters and in the fluorescence lifetime difference parameter. However, the absolute values of the parameters are different from the ones observed in flow. We attribute these differences to the different conditions the cells were exposed to for establishing their spatial confinement. Conditions in the flow experiment culture flask are closer to the environmental conditions than those in agarose, where gas diffusion is limited. Imaging, therefore, qualitatively corroborates the two-state behavior of Syn. WH8102 cells observed in flow-based measurements. Most importantly, the cell-averaged parameter values indeed represent spatially distinct cell states.

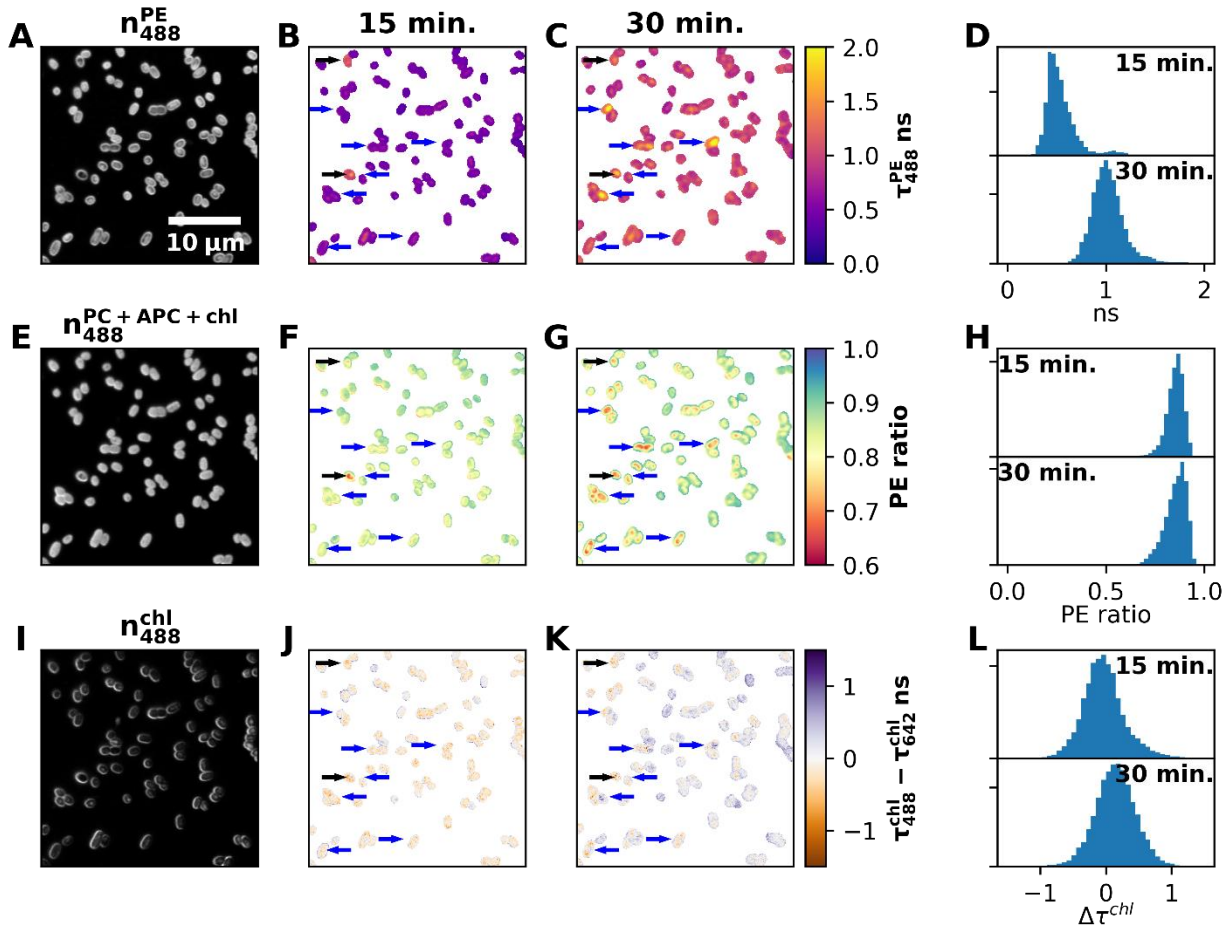

Fig. 6. Spatial distribution of parameter values in imaging of *Syn.* WH8102

Images show parameter values in Syn. WH8102 cells for τ_{488}^{PE} (B, C) PE ratio (F, G), and $\tau_{488}^{chl} - \tau_{642}^{chl}$ (J, K), 15 (B, F, J) and 30 (C, G, K) minutes into the light jump. Shown are also pixel-wise histograms of these parameter values (D, H, L). Values reported for cells with a threshold of 200 photons in the $\lambda_{ex.}$=488 nm, PC+APC+chl channel per pixel. Intensities in n_{488}^{PE}, $n_{488}^{PC+APC+chl}$, and n_{488}^{chl} channels are shown in A, E, and I respectively. Black arrows indicate selected cells with long τ_{488}^{PE}lifetimes in the 15-minute light jump condition, while blue arrows indicate selected cells with low PE ratio in the 30-minute lightjump condition.

The data observed here, on a single cell basis, exhibits a similar trend to the previously-reported bulk spectroscopic parameters of light jump experiments (*31*). Previous experiments, however, could not have resolved the distinct fluorescence-based cell-state transitions that we report here, due to ensemble averaging over multiple unsynchronized cells.

Cell state transitions in dinoflagellates

So far, we focused on phytoplankton with PBS systems. Seeking to extend our understanding to chlorophyll-based light harvesting systems, we turned our attention to the dinoflagellate *P. micans*, which uses c*hl a/c* LHCs. This requires different terminology for derived parameters (Table S1). *P. micans* display only minor changes in the mean fluorescence lifetime parameter $\boldsymbol{\tau_{488}^{chl\ a+c}}$ throughout the diurnal cycle with 6 µmol PAR (Fig. 7, A). Owing to its almost exclusive emission in the far red, most parameters based on brightnesses and their ratios, such as the excitation cross-section, show little fluctuations (Fig. 7, B, C). *P. micans* responds to light jumps with a decrease in $\boldsymbol{\tau_{488}^{chl\ a+c}}$ indicative of nonradiative dissipative processes, such as heat dissipation or non-photochemical quenching (NPQ). Lifetime values recover within 1-2 hours post light jump (Fig. 7, D). The apparent reduced flavin content is similarly perturbed during the light jump into the hour afterwards, decreasing significantly before returning to the steady-state values observed before the light jump (Fig. 7, F).

Lifetime parameters, such as $\boldsymbol{\tau_{488}^{chl\ a+c}}$, always appear as a single peak. As for the excitation cross-section, a minor yet nonegligible subpopulation is observed in the histograms throughout the experiment (fig 7, B, E). While this heterogeneity is less striking relative to that of Syn. WH8102 or *P. purp*, it nevertheless still indicates the presence of cell states.

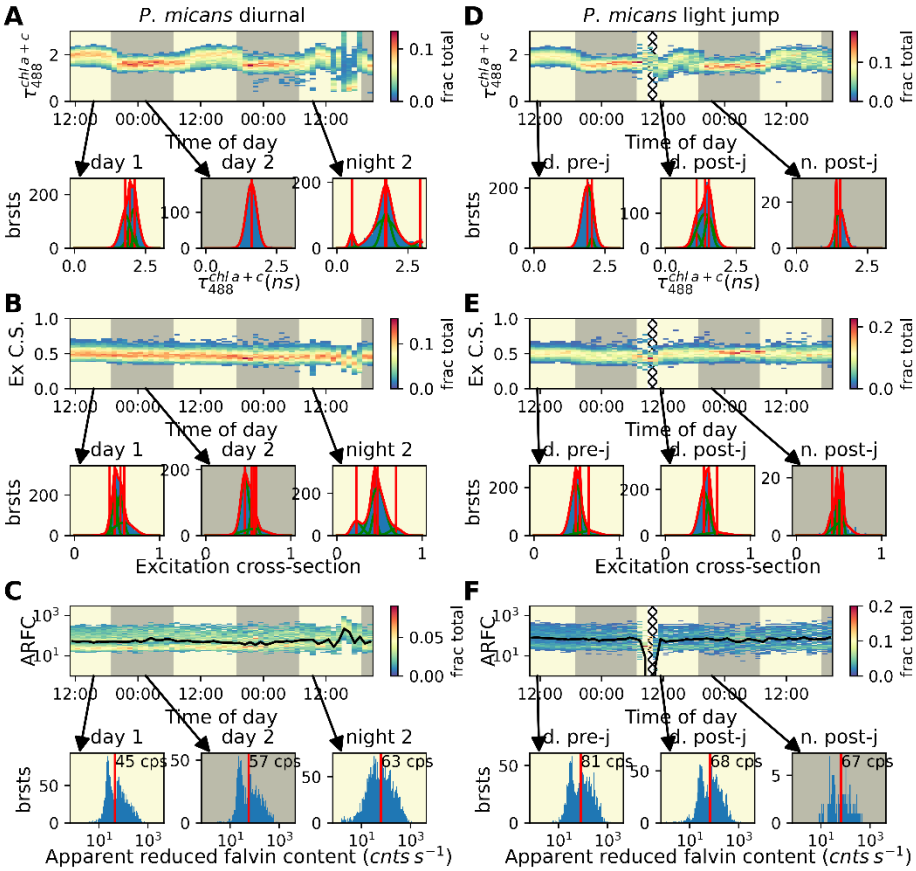

Fig. 7. *P. micans* diurnal cycle without or with a light perturbation
(A-C): Diurnal cycle. (D-F): Diurnal cycle in the presence of a light jump perturbation. Kymographs show changes in values of select parameters over time, using hour-long bins. Day and night are indicated by yellow and gray backgrounds respectively, and the period of the light perturbation is indicated by gridded background. Burst histograms of parameters in select hours are shown below each kymograph. Except for C and F, histograms are fit with sum-of-multiple-central-distributions (i.e., specific central distribution selected by parameter) with best-fit selected by F-test. Vertical red lines showing the centroids of each central distribution, and red line showing best-fit model and green lines the underlying central distributions. Parameter selection (for explanation of names see table 2) as follows (A, D) τ_{488}^{chl}, histograms fit with sum-of-multiple-Gaussians, (B, E) Excitation cross-section histograms fit with sum-of-multiple-beta-distributions, and (C, F) excitation cross-section vertical line represents mean value. Towards the end of the diurnal cycle experiment, some clogging has affected the burst rate, and hence the quality of the data.

Summary

Our results reveal photo-acclimating strategies in phytoplankton that are characterized by cell-wide coordinated state transitions. Interestingly, we found that PBS-based photosynthetic systems exhibit clearly discernible cell-states, some of which with increased fluorescence lifetime were populated only following an abrupt light perturbation. Additionally, the efficiency of the acclimation response following the light perturbation was less than 100%, as can be judged by the fraction of the high lifetime cell-states, and the recovery lasted almost a day. In chlorophyll-based photosynthetic systems, distinct cell states were observed, albeit with smaller differences between cell-state subpopulation values. Upon light perturbation, a unique cell-state with lower lifetime was populated with 100% efficiency, followed by a rapid recovery to steady-state within 1-2 hours. Indeed, using the herein presented single-cell approach uncovered novel features of light acclimation responses in different red lineage phytoplankton species.

The emergence of the long fluorescence lifetime subpopulation during the light jump in *Syn.* WH8102 indicates that the acclimation of cyanobacteria to light intensity perturbations involves a choice that occurs independently for each cell. The nonradiative excitation energy transfer-sensitized emission observed as positive values in the $\boldsymbol{\tau_{488}^{chl} - \tau_{642}^{chl}}$ parameter, combined with the increase in PE fluorescence lifetime values, further indicates that the transition is a result of PE decoupling, in whole or in part from the PBS core (*31*, *32*), which drastically reduces the rate of nonradiative excitation energy transfer. Therefore, this decoupling must be tied with a signal transduction mechanism that coordinates rapid decoupling in many photosynthetic systems across vast regions of the cell. A recent report suggests that spatio-temporal properties of cell signaling in cyanobacteria can be very robust (*33*).

P. micans adapts to light perturbations in a different way, with fluorescence lifetimes decreasing, with no indication of nonradiative excitation energy transfer-sensitized emission. Therefore, in response to a light jump these dinoflagellates must activate NPQ mechanisms that involves quenching of fluorescence instead of decoupling of antenna complexes (*34*). Evidence for two distinct populations, based on lifetime parameters, was observed to a certain extent also in the dinoflagellates.

While all tested organisms showed variability in their auto-fluorescence parameter values, we note that when taking all parameters together, each organism in each given condition occupies its own value signatures in the parameter space. This makes the approach presented in this study applicable for environmental studies. Multidimensional fluorescence parameter signatures will identify different genera, experiencing different conditions within. With so many fluorescence-based parameters, we expect to solve the inverse problem of identifying photosynthetic microorganisms and their cell photophysiological states from multidimensional parameter signatures. While the herein presented setup used two pulsed-interleaved laser excitation sources, four distinct spectral channels and three parameter type bases (i.e., fluorescence intensities, brightnesses and lifetimes), more pulsed-interleaved laser excitation sources and better spectral filtration into more distinct spectral bands, will further increase the information content, which, in turn, will further substantiate the uniqueness of multidimensional parameter signatures. Therefore, the time-resolved multiparameter single cell approach presented in this study as a basis for functional single cell physiological monitoring as response to a variety of biotic and abiotic perturbations.

Acknowledgments

Funding

Israel Science Foundation grant 556/22 (EL)
Israel Science Foundation grant 663/23 (NK)
The Racah Nano Venture Fund (NK, EL)
The Zuckerman Stem Leadership Postdoctoral Program (PDH)

Author Contributions

Conceptualization: PDH, NK, EL
Methodology: PDH, NBE
Investigation: PDH, NBE, NK, EL
Visualization: PDH, NBE
Funding acquisition: PDH, NK, EL
Project administration: NK, EL
Supervision: NK, EL
Writing – original draft: PDH, NK, EL
Writing – review & editing: PDH, NBE, NK, EL

Competing Interests

PDH, NBE, NK and EL have submitted a provisional patent on the experimental approach. Authors declare that they have no competing interests.

Data and Materials Availability

All raw data, analysis code and results are freely available over Zenodo: https://doi.org/10.5281/zenodo.10446018

References and Notes

1. M. Y. Gorbunov, P. G. Falkowski, Using Chlorophyll Fluorescence to Determine the Fate of Photons Absorbed by Phytoplankton in the World's Oceans. *Annu. Rev. Mar. Sci.* **14**, 213–238 (2022).
2. M. Stramska, T. D. Dickey, Short-term variability of the underwater light field in the oligotrophic ocean in response to surface waves and clouds. *Deep Sea Research Part I: Oceanographic Research Papers* **45**, 1393–1410 (1998).
3. A. Stirbet, D. Lazár, Y. Guo, G. Govindjee, Photosynthesis: basics, history and modelling. *Annals of Botany* **126**, 511–537 (2020).
4. T. Ikeya, K. Ohki, M. Takahashi, Y. Fujita, Photosynthetic characteristics of marine Synechococcus spp. with special reference to light environments near the bottom of the euphotic zone of the open ocean. *Marine Biology* **118**, 215–221 (1994).
5. A. W. D. Larkum, "Light-Harvesting in Cyanobacteria and Eukaryotic Algae: An Overview" in *Photosynthesis in Algae: Biochemical and Physiological Mechanisms*, A. W. D. Larkum, A. R. Grossman, J. A. Raven, Eds. (Springer International Publishing, Cham, 2020; https://doi.org/10.1007/978-3-030-33397-3_10), pp. 207–260.
6. B. R. Green, What Happened to the Phycobilisome? *Biomolecules* **9**, 748 (2019).
7. J. Ma, X. You, S. Sun, X. Wang, S. Qin, S.-F. Sui, Structural basis of energy transfer in Porphyridium purpureum phycobilisome. *Nature* **579**, 146–151 (2020).
8. E. J. Dodson, J. Ma, M. Suissa Szlejf, N. Maroudas-Sklare, Y. Paltiel, N. Adir, S. Sun, S.-F. Sui, N. Keren, The structural basis for light acclimation in phycobilisome light harvesting systems systems in Porphyridium purpureum. *Communications Biology* **6**, 1210 (2023).
9. H. Staleva-Musto, R. West, M. Trathnigg, D. Bína, R. Litvín, T. Polívka, Carotenoid–chlorophyll energy transfer in the fucoxanthin–chlorophyll complex binding a fucoxanthin acyloxy derivative. *Faraday Discuss.* **216**, 460–475 (2019).
10. R. Nagao, K. Kato, M. Kumazawa, K. Ifuku, M. Yokono, T. Suzuki, N. Dohmae, F. Akita, S. Akimoto, N. Miyazaki, J.-R. Shen, Structural basis for different types of hetero-tetrameric light-harvesting complexes in a diatom PSII-FCPII supercomplex. *Nat Commun* **13**, 1764 (2022).
11. S. Akimoto, S. Takaichi, T. Ogata, Y. Nishimura, I. Yamazaki, M. Mimuro, Excitation energy transfer in carotenoid-chlorophyll protein complexes probed by femtosecond fluorescence decays. *Chemical Physics Letters* **260**, 147–152 (1996).
12. T. Schulte, D. M. Niedzwiedzki, R. R. Birge, R. G. Hiller, T. Polívka, E. Hofmann, H. A. Frank, Identification of a single peridinin sensing Chl-a excitation in reconstituted PCP by crystallography and spectroscopy. *Proceedings of the National Academy of Sciences* **106**, 20764–20769 (2009).
13. Z. Kvíčalová, J. Alster, E. Hofmann, P. Khoroshyy, R. Litvín, D. Bína, T. Polívka, J. Pšenčík, Triplet–triplet energy transfer from chlorophylls to carotenoids in two antenna complexes from dinoflagellate Amphidinium carterae. *Biochimica et Biophysica Acta (BBA) - Bioenergetics* **1857**, 341–349 (2016).
14. C. Büchel, Light harvesting complexes in chlorophyll c-containing algae. *Biochimica et Biophysica Acta (BBA) - Bioenergetics* **1861**, 148027 (2020).

15. B. B. Prézelin, H. A. Matlick, Time-course of photoadaptation in the photosynthesis-irradiance relationship of a dinoflagellate exhibiting photosynthetic periodicity. *Marine Biology* **58**, 85–96 (1980).
16. H. Lin, F. I. Kuzminov, J. Park, S. Lee, P. G. Falkowski, M. Y. Gorbunov, The fate of photons absorbed by phytoplankton in the global ocean. *Science* **351**, 264–267 (2016).
17. J. Sherman, M. Y. Gorbunov, O. Schofield, P. G. Falkowski, Photosynthetic energy conversion efficiency in the West Antarctic Peninsula. *Limnology & Oceanography* **65**, 2912–2925 (2020).
18. Y. Kolodny, Y. Avrahami, H. Zer, M. J. Frada, Y. Paltiel, N. Keren, Phycobilisome light-harvesting efficiency in natural populations of the marine cyanobacteria Synechococcus increases with depth. *Commun Biol* **5**, 727 (2022).
19. R. M. Clegg, *Fret and FLIM Techniques* (Elsevier, 2009; http://www.sciencedirect.com/science/article/pii/S0075753508000016)vol. 33 of *Laboratory Techniques in Biochemistry and Molecular Biology*.
20. S. Nozue, A. Mukuno, Y. Tsuda, T. Shiina, M. Terazima, S. Kumazaki, Characterization of thylakoid membrane in a heterocystous cyanobacterium and green alga with dual-detector fluorescence lifetime imaging microscopy with a systematic change of incident laser power. *Biochimica et Biophysica Acta (BBA) - Bioenergetics* **1857**, 46–59 (2016).
21. I. Iermak, J. Vink, A. N. Bader, E. Wientjes, H. Van Amerongen, Visualizing heterogeneity of photosynthetic properties of plant leaves with two-photon fluorescence lifetime imaging microscopy. *Biochimica et Biophysica Acta (BBA) - Bioenergetics* **1857**, 1473–1478 (2016).
22. A. F. Bhatti, D. Kirilovsky, H. Van Amerongen, E. Wientjes, State transitions and photosystems spatially resolved in individual cells of the cyanobacterium *Synechococcus elongatus*. *Plant Physiology* **186**, 569–580 (2021).
23. X. J. Zhang, Y. Fujita, R. Tokutsu, J. Minagawa, S. Ye, Y. Shibata, High-Speed Excitation-Spectral Microscopy Uncovers In Situ Rearrangement of Light-Harvesting Apparatus in *Chlamydomonas* during State Transitions at Submicron Precision. *Plant and Cell Physiology* **62**, 872–882 (2021).
24. D. Verhoeven, H. Van Amerongen, E. Wientjes, Single chloroplast in folio imaging sheds light on photosystem energy redistribution during state transitions. *Plant Physiology* **191**, 1186–1198 (2023).
25. M. Zubik-Duda, R. Luchowski, M. Maksim, A. Nosalewicz, P. Zgłobicki, A. K. Banaś, W. Grudzinski, W. I. Gruszecki, The photoprotective dilemma of a chloroplast: to avoid high light or to quench the fire? *The Plant Journal* **115**, 7–17 (2023).
26. M. E. Blaha, S. Hasan, C. Dusny, D. Belder, Fluorescence lifetime activated droplet sorting (FLADS) for label-free sorting of *Synechocystis* sp. PCC6803. *Lab Chip* **22**, 1604–1614 (2022).
27. G. Dishon, Z. Dubinsky, M. Fine, D. Iluz, Underwater light field patterns in subtropical coastal waters: A case study from the Gulf of Eilat (Aqaba). *Israel Journal of Plant Sciences* **60**, 265–275 (2012).
28. C. Six, J. C. Thomas, B. Brahamsha, Y. Lemoine, F. Partensky, Photophysiology of the marine cyanobacterium Synechococcus sp. WH8102, a new model organism. *Aquatic Microbial Ecology* **35**, 17–29 (2004).
29. B. K. Müller, E. Zaychikov, C. Bräuchle, D. C. Lamb, Pulsed Interleaved Excitation. *Biophysical journal* **89**, 3508–3522 (2005).

30. C. A. Reissaus, K. H. Day, R. G. Mirmira, K. W. Dunn, F. M. Pavalko, R. N. Day, PIE-FLIM Measurements of Two Different FRET-Based Biosensor Activities in the Same Living Cells. *Biophysical Journal* **118**, 1820–1829 (2020).
31. N. Bezalel-Hazony, H. Zer, S. Nathanson, S. Shevtsov-Tal, O. Ostersetzer-Biran, N. Keren, Functional flexibility of cyanobacterial light harvesting phycobilisomes enable acclimation to the complex light regime of mixing marine water columns. *The FEBS Journal* **290**, 400–411 (2023).
32. P. I. Calzadilla, D. Kirilovsky, Revisiting cyanobacterial state transitions. *Photochemical & Photobiological Sciences* **19**, 585–603 (2020).
33. Arbel-Goren Rinat, Dassa Bareket, Zhitnitsky Anna, Valladares Ana, Herrero Antonia, Flores Enrique, Stavans Joel, Spatio-temporal coherence of circadian clocks and temporal control of differentiation in Anabaena filaments. *mSystems* **0**, e00700-23 (2023).
34. T. Lacour, M. Babin, J. Lavaud, Diversity in Xanthophyll Cycle Pigments Content and Related Nonphotochemical Quenching (NPQ) Among Microalgae: Implications for Growth Strategy and Ecology. *Journal of Phycology* **56**, 245–263 (2020).